VOL. 16, NO. 2, JANUARY 2021 ISSN 1819-6608
ARPN Journal of Engineering and Applied Sciences

www.arpnjournals.com

MICROSCOPE IMAGE SEGMENTATION OF PHOTO LITHOGRAPHIC MASKS

Udomchok Phromsuwan[1], Chitnarong Sirisathitkul[1] and Yaowarat Sirisathitkul[2]
[1]School of Science, Walailak University, Nakhon Si Thammarat, Thailand
[2]School of Engineering and Technology, Walailak University, Nakhon Si Thammarat, Thailand
E-Mail: kinsywu@gmail.com

ABSTRACT

Digital image processing is increasingly influential in the inspection of industrial products. For microelectronic industry, the pattern examination required for photolithographic masks can be facilitated by the image segmentation. This work demonstrates that arrays of rectangular chromium films on photolithographic masks are effectively detected by the gradient-based edge detection. The RGB micrographs are successively converted to grayscale and binary images. The closing morphology algorithm is then applied to reduce noise in the images before the application of the Canny edge detector. After subsequent steps of fill area and remove small objects, the area of each rectangle can then be computed. This image processing procedure gives rise to less than 0.8% difference from the one-by-one inspection and the ratios of rectangular areas confirmed the high accuracy. The standard deviations in number of pixels averaged from 10-17 rectangles in three images are 0.81-1.89% indicating the precision of photolithography and image processing. The brightness used in this optical microscopy has no apparent effect but the precision and accuracy are significantly reduced in the image with low magnification and different illumination.

Keywords: image processing, photolithographic mask, optical microscopy, canny edge detector.

1. INTRODUCTION

Digital image processing is increasingly used with images for a variety of purposes including medical diagnosis, geographical analysis, engineering inspection and material characterization. Image segmentation is the most important process to separate interesting objects from the background. The segmentation process consists of the grouping of the object pixels and the edge pixels [1]. In the gradient-based edge detection, the intensity in the image is measured and the contours with large intensity gradients are identified as the edge of objects. Edge detection is used to detect the boundaries between objects and background. Pixels representing the object can then be analyzed once their boundaries are located.

In the satellite image, various geographical features such as craters can be detected by using the circular Hough transform edge detection [2]. With the magnetic resonance imaging (MRI), the segmentation process is carried out to extract the features for the tumor classification [3] and to quantify of cartilage thickness for knee osteoarthritis [4]. In the diabetic retinopathy, the FCM algorithm is used to detect the secretion of retinal images [5]. In addition to radiological and histopathological images, fluorescence microscope images are often analyzed in clinical applications [6]. Acid-fast bacilli in bacilloscopies can be detected and counted to diagnose pulmonary tuberculosis (TB) [7]. In the ultrasonography examination, the age of the fetus and uterine diameter from low-resolution image were measured by employing the image morphology and edge detection in the segmentation process [8].

In the machine vision system, the dark spots, molds or peeling skin of mangoes were identified by using the edge detection [9]. A Canny edge detector was also used to extract the edges of the recyclable materials for waste classification by a machine vision system [10]. In rice grading, the rice internal cracks were examined with different methods of the edge detection to differentiate and the degree level of rice were analyzed [11]. In marker-based augmented reality, edge detections such as Roberts cross operator, Sobel operators and Prewitt operators were used for reading and detecting the edge in the marker [12].

Image processing is effectively implemented on optical microscope images for material characterizations. Examples are crack inspections on concrete by using the pixel intensity distribution [13] and metallurgical process monitoring by using the adaptive median filter with local contrast enhancement [14]. For electron microscope images, a large number of nano- and microscopic objects can rapidly be assessed by electron microscope image processing with superior accuracy to one-by-one human inspections [1], [15-17]. It is suggested that a similar procedure can be used for both scanning electron microscope (SEM) and transmission electron microscope (TEM) images [18].

Microelectronic devices are fabricated by the process of masked irradiation. A photoresist layer is coated on a silicon wafer, then partially covered by the mask and finally irradiated by ultraviolet light to transfer pattern in photolithography. Repeated features have usually been implemented as array of sensing, magnetic and photonic elements. Since any deviations in shape and position from regular patterns inevitably affect physical properties of the devices, inspections of lithographic mask and pattern are mandatory. Image processing effectively examined defects in structures patterned by laser beam [19], electron beam [20] and nanoimprint lithography [21].

In this work, optical micrographs of photolithographic masks are analyzed by imaging processing to increase accuracy and decrease time of the inspections. Adapted from the procedure used with SEM and TEM images [16, 17], features in microscope images

were extracted from the background by the gradient-based edge detection. The Canny operator is selected based on the comparison with Laplacian of Gaussian, Roberts Cross, Prewitt and Sobel edge detectors and previously implemented in pattern inspection of X-ray lithographic pores in SEM [16] and self-assembled nanoparticles in TEM [17] images.

2. MATERIALS AND METHODS

Three chromium-coated glass plates were patterned by the photolithography. Each lithographic mask comprised arrays of 100×30 μm^2 chromium films alternated with smaller (10×30 μm^2) ones. The width of the gap between large and small rectangles is varied as 2, 16 and 32 μm. six microscopic images were taken by an optical microscopy (Nikon Eclipse ME660L) and used as test images. Figure-1a was taken from the first mask (2 μm gaps) by adjusting the illumination to enhance visibility of smaller rectangles. Figure-1b to Figure-1d is from the same mask with 16 μm gaps between the rectangles. For the third mask (32 μm gaps), the brightness was varied in photographing Figure-1e and Figure-1f. All images were in .jpg format with the resolution of 1280×960 pixels.

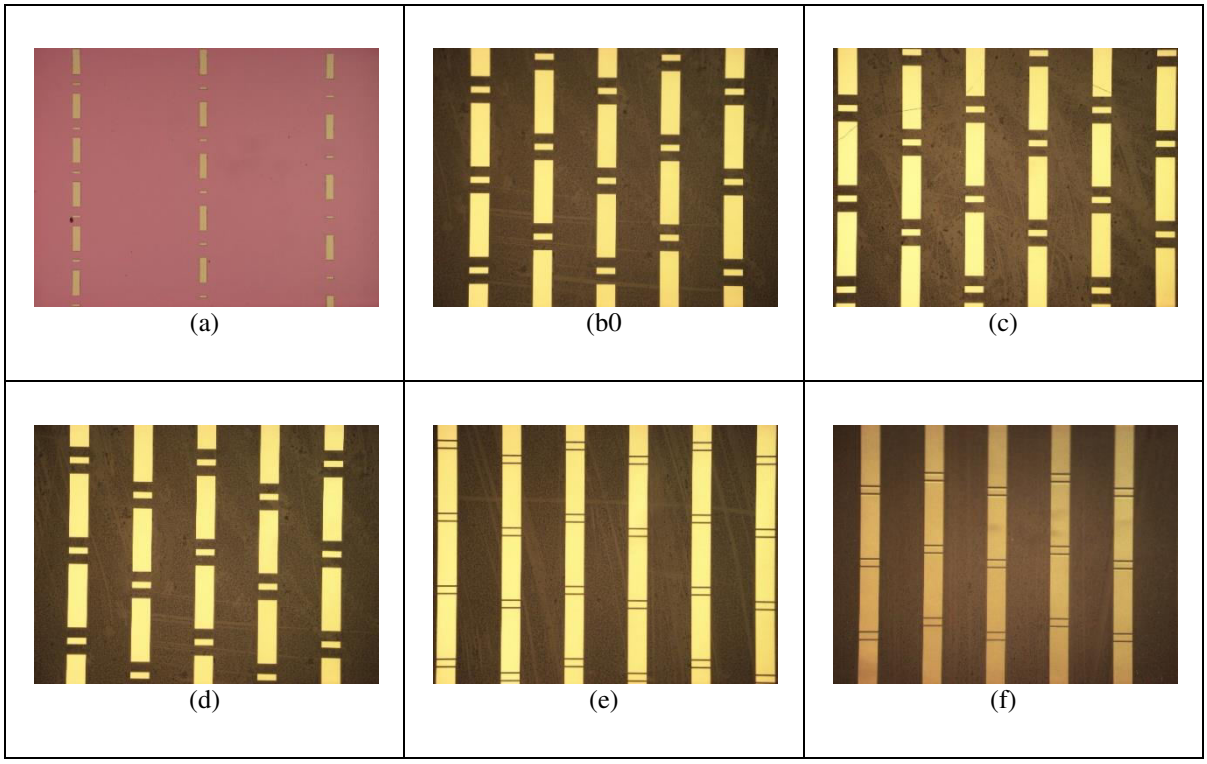

Figure-1. Six test images of three photolithographic masks obtained by optical microscopy.

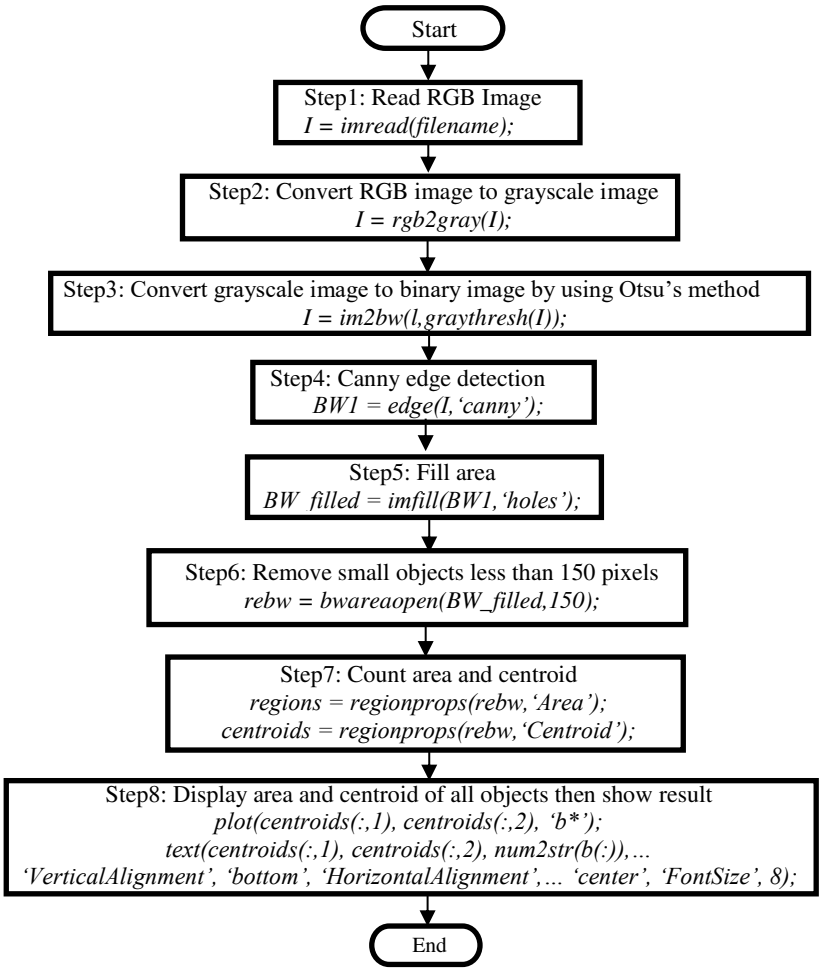

Figure-2. Flowchart with MATLAB script for gradient-based edge detection.

The microscope image processing procedure operated on MATLAB 7.11 (R2010b) is summarized in Figure-2. The initial step was to convert the RGB inputs into grayscale images. Each grayscale image was then transformed to a binary image by using the Otsu's thresholding. The threshold value was derived from the intensity difference between the chromium and the glass areas. Each individual rectangle was then detected by using the Canny edge detector in the Image Processing Toolbox of MATLAB. The detected outputs from the edge detector were then filled because the intensity of pixels surrounding them was non-uniform. The pixel was added from one side to the other until the area was enclosed by pixels of comparable intensity. Subsequently, the small unfilled objects of less than 150 pixels were removed. Incomplete rectangles on the top and bottom of the images are omitted. Finally, the number of detections and the detected area of each chromium rectangle were determined.

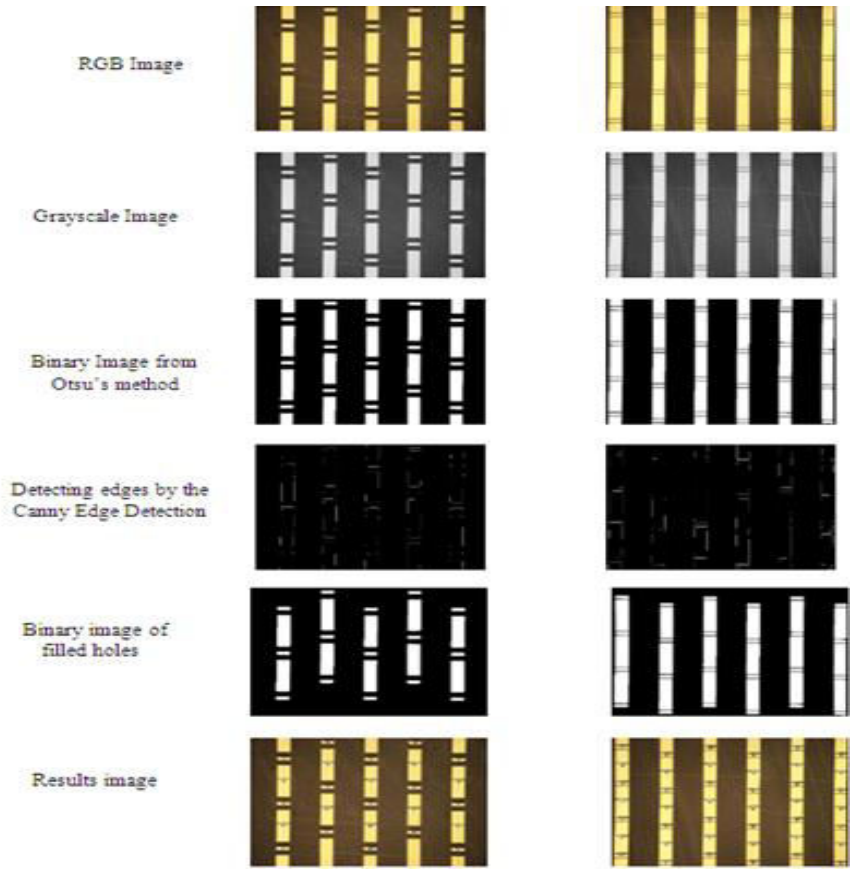

Figure-3. Outputs from each stage in microscope image processing of (a) Figure-1b and (b) Figure-1e.

3. RESULTS AND DISCUSSIONS

The outputs from image processing of Figures-1b and Figures-1e are successively shown in Figure-3. The conversion from grayscale to binary image provides a high contrast between black objects and the white background according to the global thresholding value obtained by the Otsu's method. The output from the Canny edge detection shows the edges as white pixels and the rest in black. All rectangular chromium films in every micrograph are detected with some discontinuity. The areas become white area after filling process and noises are eliminated in the small object removal. The center is identified and the area is computed for each rectangular chromium film in final results.

Table-1. Areas of rectangular chromium films averaged from microscope image processing.

Image	Small rectangles (10×30 μm^2)		Large rectangles (100×30 μm^2)		The ratio of large to small rectangles
	Number	Average Area (Pixels)	Number	Average Area (Pixels)	
1a ---	15 ---	215±18 ---	15 ---	2599±64 ---	12.08 ---
1b	15	1691±32	10	16977±150	10.04
1c	17	1693±23	12	17010±215	10.05
1d ---	15 ---	1691±15 ---	10 ---	16935±138 ---	10.01 ---
1e	24	1664±32	18	16984±194	10.21
1f	15	1676±44	10	16983±95	10.13

The pixels of detected islands were averaged and shown with standard deviations in Table-1. Firstly, Figure-1b to Figure-1d from the same mask under the same illumination is compared. The average areas of small rectangles in three images are nearly equal ranging between 1691-1693 pixels. To assess the accuracy of the

method, these values are compared to the one-by-one inspection. The number from the manual pixel counting is 1680. The areas of larger rectangles are also accurately determined by the image processing with only 0.1-0.3% difference from the one-by-one inspection. Moreover, the ratios of large to small rectangles are remarkably close to 10. For each image, the standard deviations in the range of 0.81-1.89% indicate the precision of photolithography and microscope image processing.

In the case of Figure-1e and Figure-1f, the precision is not much varied by the difference in brightness. Image processing results in shown Table-1 are close to the one-by-one inspections of both large (16992 pixels) and small (1656 pixels) rectangles. The ratios of large to small rectangles, slightly higher than those obtained from Figure-1b to Figure-1d, from both methods are in very good agreement. Interestingly, the largest ratio over 12 obtained from image processing of Figure-1a significantly differs from the expected value (10) and the one-by-one inspection (11.5). A substantial decrease in accuracy is likely due to the lowest magnification which also results in the large standard deviations in both large (2.46%) and small (8.37%) areas in this image. The low magnification was used to cover a comparable number of rectangles separated by very large gaps. Small rectangles are not clearly separated from the background and the efficiency of edge detector is predictably reduced. In the case of micrographs with low contrast, the preprocessing is required prior to the intensity-based image segmentation. To enhance the contrast during the inspection by the optical microscope, a different illumination Figure-1a is used but become another source of the reduction in precision and accuracy. Highly magnified images, albeit with smaller number of objects, are preferred in the characterization by the gradient-based edge detection.

4. CONCLUSIONS

Optical micrographs of photolithographic masks were efficiently analyzed using image processing process. With the incorporation of Canny edge detector in MATLAB, images of rectangular partially etched chromium films on glass plates are captured and the area can be computed to assess the pattern deviations. The thresholding, edge detection, hole filling and area opening steps are also needed to reduce noise and construct the shape of all objects in the image. The photolithography and image processing in this work were highly reproducible. The precision and accuracy were significantly reduced in the case of image with low magnification and different illumination.

ACKNOWLEDGEMENT

This work was financially supported by the Industry/University Cooperative Research Center (I/UCRC) in HDD Component, the Faculty of Engineering, Khon Kaen University and National Electronics and Computer Technology Center, National Science and Technology Development Agency with the approval of Seagate Technology (Thailand). This project was partially supported by the New Strategic Research (P2P) project, Walailak University, Thailand.

REFERENCES

[1] L. Wu, Y. R. Chen, J. X. Guo and F. Wang. 2020. Electron microscope system image acquisition information processing. Acta Microscopica. 29(1): 303-312.

[2] Md. H. Sharif, S. Uyaver and Z. Zerdo. 2018. Classification and detection of various geographical features from satellite imagery. Periodicals of Engineering and Natural Sciences. 6(1)1: 84-94.

[3] S. Kumar, D. Jayadevappa and M. V. Shetty. 2018. A novel approach for segmentation and classification of brain MR images using cluster deformable based fusion approach. Periodicals of Engineering and Natural Sciences. 6(2): 237-242.

[4] M. K. Lakshmi and N. Prabakaran. 2015. Automatic detection of cartilage thickness for early detection of Koa. ARPN Journal of Engineering and Applied Sciences. 10(7): 3112-3115.

[5] M. Q. Jawad, M. A. Yousif and D. H. Abbas. 2019. Assess the performance of the diagnosis ways of diabetic retinopathy. Periodicals of Engineering and Natural Sciences. 7(3): 1383-1395.

[6] Y. Y. Xu and H. B. Shen. 2020. Review of research on biomedical image processing based on pattern recognition. Journal of Electronics & Information Technology. 42(1): 201-213.

[7] J. L. Diaz-Huerta, A. D. Tellez-Anguiano, M. A. Fraga-Aguilar, J. A. Gutierrez-Gnecchi and S. Arellano-Calderon. 2019. Image processing for AFB segmentation in bacilloscopies of pulmonary tuberculosis diagnosis. PLOS One. 14(7): e0218861.

[8] R. Supriyanti, A. A. Hafidh, Y. Ramadhani and H. B. Widodo. 2018. Measuring gestational age and uterine diameter based on image segmentation. ARPN Journal of Engineering and Applied Sciences. 13(2): 670-676.

[9] A. D. M. Africa, E. C. Del Rosario, J. V. G. Legal and R. M. C. Manuel. 2019. Development of a machine vision system for quality control of fruits Africa. ARPN Journal of Engineering and Applied Sciences. 14(23): 4086-4092.

[10] A. D. M. Africa, N. P. J. Labay, M. S. B. Ong, J. A. J. Sales and M. M. E. Toyoda. 2019. Vision-based algorithm for recyclable waste classification. ARPN Journal of Engineering and Applied Sciences. 14(13): 2459-2463.

[11] W. P. N. W. M. Tahir, N. Hussin, Z. Z. Htike and W. Y. N. Naing. 2015. Rice grading using image processing. ARPN Journal of Engineering and Applied Sciences. 10(21): 10131-10137.

[12] S. P. A. H. Pandiangan, T. W. Purboyo and R. E. Saputra. 2019. A review of edge image detection for marker-based augmented reality. ARPN Journal of Engineering and Applied Sciences. 14(17): 3088-3095.

[13] Y. Vashpanov, J. Y. Son, G. Heo, T. Podousova and Y. S. Kim. 2019. Determination of geometric parameters of cracks in concrete by image processing. Advances in Civil Engineering. 2019: article no. 2398124.

[14] B. H. Yin. 2020. Metallurgical process monitoring under microscope image analysis. Acta Microscopica. 29(2): 614-625.

[15] N. Bonnet. 2004. Some trends in microscope image processing. Micron. 35: 635-653.

[16] U. Phromsuwan, Y. Sirisathitkul, C. Sirisathitkul, P. Muneesawang and B. Uyyanonvara. 2013. Quantitative Analysis of X-ray Lithographic Pores by SEM Image Processing. MAPAN-Journal of Metrology Society of India. 28(4): 327-333.

[17] Y. Sirisathitkul, P. Sarmphim and C. Sirisathitkul. 2020. Surface coverage and size analysis of redispersed nanoparticles by image processing. Particulate Science and Technology. https://doi.org/10.1080/02726351.2020.1758260.

[18] D. Saladra and M. Kopernik. 2016. Qualitative and quantitative interpretation of SEM image using digital image processing. Journal of Microscopy. 264(1): 102-124.

[19] D. A. Belousov, A. V. Dostovalov, V. Korolkov, and S. L. Mikerin. 2019. A microscope image processing method for analyzing TLIPSS structures. Computer Optics. 43(6): 936-945.

[20] E. Kratschmer, D. P. Klaus, R. Viswanathan, M. L. Turnidge, P. L. Reed and B. McPhail. 2009. Image processing using shape recognition for alignment to damaged registration marks in electron beam lithography. Journal of Vacuum Science and Technology B. 27(6): 2563-2568.

[21] D. Pietroy, I. Gereige and C. Gourgon. 2013. Automatic detection of NIL defects using microscopy and image processing. Microelectronic Engineering. 112(SI): 163-167.